Synthesis of hydrogenated diamondlike carbon thin films using neon–acetylene based high power impulse magnetron sputtering discharges

Asim AijazSascha LouringDaniel LundinTomáš KubartJens Jensen, Kostas Sarakinos, and Ulf Helmersson

Citation: Journal of Vacuum Science & Technology A: Vacuum, Surfaces, and Films **34**, 061504 (2016); doi: 10.1116/1.4964749

View online: http://dx.doi.org/10.1116/1.4964749

View Table of Contents: http://avs.scitation.org/toc/jva/34/6

Published by the American Vacuum Society

Synthesis of hydrogenated diamondlike carbon thin films using neon–acetylene based high power impulse magnetron sputtering discharges

Asim Aijaz[a)]
Department of Physics, Chemistry and Biology, IFM-Material Physics, Linköping University, SE-581 83 Linköping, Sweden and Department of Engineering Sciences, The Ångström Laboratory, Uppsala University, P.O. Box 534, SE-751 21 Uppsala, Sweden

Sascha Louring
Interdisciplinary Nanoscience Center (iNANO), Aarhus University, Ny Munkegade 120, 8000 Aarhus C, Denmark and Tribology Centre, Danish Technological Institute, Teknologiparken, Kongsvang Allé 29, DK-8000 Aarhus C, Denmark

Daniel Lundin
Laboratoire de Physique des Gaz et Plasmas-LPGP, UMR 8578 CNRS, Université Paris-Sud, Université Paris-Saclay, 91405 Orsay Cedex, France

Tomáš Kubart
Department of Engineering Sciences, The Ångström Laboratory, Uppsala University, P.O. Box 534, SE-751 21 Uppsala, Sweden

Jens Jensen, Kostas Sarakinos, and Ulf Helmersson
Department of Physics, Chemistry and Biology, IFM-Material Physics, Linköping University, SE-581 83 Linköping, Sweden

(Received 7 July 2016; accepted 27 September 2016; published 10 October 2016)

Hydrogenated diamondlike carbon (DLC:H) thin films exhibit many interesting properties that can be tailored by controlling the composition and energy of the vapor fluxes used for their synthesis. This control can be facilitated by high electron density and/or high electron temperature plasmas that allow one to effectively tune the gas and surface chemistry during film growth, as well as the degree of ionization of the film forming species. The authors have recently demonstrated by adding Ne in an Ar-C high power impulse magnetron sputtering (HiPIMS) discharge that electron temperatures can be effectively increased to substantially ionize C species [Aijaz *et al.*, Diamond Relat. Mater. **23**, 1 (2012)]. The authors also developed an Ar-C_2H_2 HiPIMS process in which the high electron densities provided by the HiPIMS operation mode enhance gas phase dissociation reactions enabling control of the plasma and growth chemistry [Aijaz *et al.*, Diamond Relat. Mater. **44**, 117 (2014)]. Seeking to further enhance electron temperature and thereby promote electron impact induced interactions, control plasma chemical reaction pathways, and tune the resulting film properties, in this work, the authors synthesize DLC:H thin films by admixing Ne in a HiPIMS based Ar/C_2H_2 discharge. The authors investigate the plasma properties and discharge characteristics by measuring electron energy distributions as well as by studying discharge current characteristics showing an electron temperature enhancement in C_2H_2 based discharges and the role of ionic contribution to the film growth. These discharge conditions allow for the growth of thick ($>1\,\mu$m) DLC:H thin films exhibiting low compressive stresses ($\sim$0.5 GPa), high hardness ($\sim$25 GPa), low H content ($\sim$11%), and density in the order of 2.2 g/cm^3. The authors also show that film densification and change of mechanical properties are related to H removal by ion bombardment rather than subplantation. © *2016 American Vacuum Society*. [http://dx.doi.org/10.1116/1.4964749]

I. INTRODUCTION

Hydrogenated diamondlike carbon (DLC:H) thin films exhibit a wide range of properties such as low friction coefficient, chemical inertness, high refractive index, etc.,[1,2] which make them attractive for a number of industrial applications.[1,2] The properties of DLC:H depend on their structure, bonding configuration (sp^3/sp^2 fraction), and chemical composition (H content).[2] These properties can be tailored by controlling energy and composition of the film forming flux. This can be, in turn, facilitated by high electron density and electron temperature based plasma processes that allow one to effectively control the plasma and growth chemistry by generating large amount of ionized species. Examples of such processes include filtered cathodic vacuum arc, pulsed laser deposition (PLD), plasma-enhanced chemical vapor deposition (PECVD) and high power impulse magnetron sputtering (HiPIMS).[2–9]

HiPIMS operates at 2–3 orders of magnitude higher plasma density as compared to standard direct current magnetron sputtering which facilitates the generation of large ionized fraction of the deposition species.[10–12] Moreover, owing to the fact that it is based on magnetron sputtering,[10–12] HiPIMS

a)Author to whom correspondence should be addresses; electronic mail: asim.aijaz@angstrom.uu.se

is an industrially relevant method for large scale production of coatings. The potential of HiPIMS has been explored for the production of DLC thin films by several authors and it has shown promising results.[13–18] However, conventional Ar-C HiPIMS discharges have been found to exhibit significantly smaller degree of ionization of sputtered material[14] as opposed to their Ar-metal counterparts[19,20] rendering HiPIMS insufficient for synthesizing high quality DLC films. We have recently addressed this challenge[21] by developing a novel Ne-based HiPIMS process; the presence of Ne as a sputtering gas resulted in a substantial increase of the electron temperature as compared to Ar-based HiPIMS process. This led to the generation of large ionized fraction of C with relatively high C ion energies allowing for the growth of ultradense, hydrogen free DLC thin films. In particular, DLC films with mass densities in the order of 2.8 g/cm^3 were synthesized which are close to the best films obtained using state-of-the art methods for DLC production, for example, the PLD process.

We also explored a HiPIMS-based route for high-rate synthesis of dense and hard hydrogenated DLC thin films by admixing C_2H_2 into Ar ambient.[22] The presence of C_2H_2 introduced additional interactions of plasma electrons leading to dissociation and ionization of C_2H_2 along with the interactions of plasma electrons with the buffer gas and sputtered C. This process facilitated an increased amount of deposited C (tenfold increased deposition rates), and the resulting films exhibited hardness higher than 25 GPa and mass densities in the order of 2.32 g/cm^3. The promising prospect of the resulting DLC:H films was their low H content which did not exceed 10 at. %. Such a low H content together with a hardness in the order of 25 GPa and significantly high deposition rates are promising since a hydrocarbon based process (including magnetron sputtering and PECVD) typically results in H contents above 20 at. % and hardness in the range of 10–15 GPa.[2,5]

In the present work, we are adding Ne to the Ar/C_2H_2 HiPIMS discharge, which may facilitate an increased electron temperature, and hence increased ionization of depositing species, similar to our previous work in Ne + Ar discharges.[21] We synthesize thin films using Ne + Ar based C_2H_2 process and investigate the correlation between plasma and film properties. In order to elucidate the effect of admixing Ne in Ar and Ar/C_2H_2 atmosphere, we also compare the resulting film properties with our previous studies.[21,22] The plasma properties are investigated by measuring electron energy distribution functions (EEDF) (thereby determining electron temperature and electron density from EEDF), which, contrary to our expectations, shows that higher electron temperatures are obtained when the process gas (Ne + Ar) contains C_2H_2. The plasma properties are also investigated by studying the behavior of the discharge current under different gas phase composition. It is found that larger peak currents indicating the presence of larger amounts of ions are obtained for Ne + Ar/C_2H_2 discharge as compared to Ne + Ar discharge. The correlation between the plasma properties and the resulting thin films is studied by investigating the chemical composition, structural (mass density and bond configuration), and mechanical (hardness and compressive stresses) properties of the films. It is shown that the film densification (and corresponding increase in film hardness) is caused by H removal rather than subplantation of C.

II. EXPERIMENTAL DETAILS

Experiments were performed in a stainless steel vacuum chamber 420 mm in diameter and 300 mm in height that was evacuated to a base pressure below 2×10^{-4} Pa. A carbon disk 50 mm in diameter and 3 mm in thickness (purity 99.9%) was used as a sputtering target, which was mounted on a circular unbalanced magnetron. Plasma discharges were obtained using a mixed Ne, Ar, and C_2H_2 ambient under two different conditions; (1) using a gas mixture consisting of 62% Ne, 36% Ar, and 2% C_2H_2 at a total pressure of 2 Pa and (2) using a gas mixture consisting of 83% Ne, 15% Ar, and 2% C_2H_2 at a total pressure of 3.3 Pa where the gas fractions used in (1) and (2) are in pressure %. Ar was used for stabilizing the discharge owing to the difficulty encountered in igniting and obtaining a stable discharge with only Ne mixed with C_2H_2. At the higher pressure of 3.3 Pa, the discharge was comparatively more stable; therefore, a lower fraction of Ar (15%) was used.

A pulsing unit (home-built) fed by an MDX 1 K direct current generator (Advanced Energy) was used as HiPIMS power source. The power source provided unipolar rectangular shaped negative voltage pulses with variable pulsing frequencies and pulse widths. Power to the cathode was supplied using a voltage pulse of 600 Hz and pulse on time of 25 μs which resulted in a duty cycle of 1.5%. An average power of 42 W was used during all experiments. The power of 42 W was chosen after process optimization for a stable operation. The discharge voltage, U_D, and discharge current, I_D, were monitored and recorded on a Tektronix TDS2004B oscilloscope. For reference, plasma discharges using the same flow rates of Ar and Ne as specified in (1) and (2) but without C_2H_2 were obtained. Since partial pressure of C_2H_2 with 2% of the total pressure is very small (0.04 and 0.06 Pa for total working pressures of 2 and 3.3 Pa, respectively), we therefore consider that the change in Ar and Ne fractions in terms of pressure for reference discharges change only slightly and hence can be regarded as the same. From these discharges, U_D and I_D were recorded, and plasma parameters (see Sec. II A) were measured.

A. Plasma characterization

The plasma parameters, plasma density and electron temperature, were determined by measuring current–voltage characteristics of the plasma discharges using a home-built Langmuir probe measurement setup. A thin, cylindrical tungsten wire encapsulated in a ceramic tube with a protruding probe tip of length 5 mm and diameter 125 μm was used as the Langmuir probe. The probe was mounted through a side port of the chamber such that it was lengthwise parallel to the target surface. The distance between the target surface and the probe was kept fixed at 60 mm, while the tip of the probe was positioned at the center axis of the magnetron

during the measurements. The current–voltage characteristics were obtained by applying a bias potential (from −40 to +20 V in steps of 0.02 V) to the probe and recording the current drawn from the plasma. In order to take into account the temporal variation associated with the pulsed nature of the HiPIMS discharge, a time resolved current, synchronized with the cathode voltage pulse, was measured. The current was recorded in 500 time-steps each with an interval of 320 ns, giving a time-resolved current measured over a total time of 160 μs after the pulse initiation. A current–voltage characteristic curve was constructed for each time step which was used for the determination of the EEDF (denoted as g_e) using the Druyvesteyn formula[23]

$$g_e = \frac{2m}{e^2 A_{pr}} \left(\frac{2eU}{m}\right)^{1/2} \frac{d^2 I_e}{dU^2}, \tag{1}$$

where A_{pr} is the area of the probe, m and e are the mass and charge of an electron, respectively, and I_e is the electron current that is extracted from the measured probe current. U is the probe potential, which is defined with respect to the plasma potential (U_{pl}) and probe bias potential (U_{pr}) as $U = U_{pl} - U_{pr}$. It should be noted that Eq. (1) involves a second order derivative of the measured current. This means that any noise present in the data is likely to be amplified during the differentiation, thus affecting the signal-to-noise ratio. A noise suppression of the measured current was therefore performed using Blackman window filtration. The details of this method can be found elsewhere.[24]

From the EEDF, the electron density, n_e, was determined as

$$n_e = \int_0^\infty g_e(E) dE, \tag{2}$$

whereas effective electron temperature, T_{eff}, was determined via the average electron energy, E_{avg}

$$E_{avg} = \frac{1}{n_e} \int_0^\infty E g_e(E) dE, \tag{3}$$

using the relation

$$T_{eff} = \frac{2}{3} E_{avg}. \tag{4}$$

B. Film synthesis and characterization

Films were deposited under the two conditions [(1) and (2)] described above on single crystalline Si (100) substrates mounted on a water cooled stationary substrate holder placed at a distance of 60 mm from the target surface. Prior to depositions, the substrates were ultrasonically cleaned using acetone and isopropanol for 5 min each and blow dried using dry nitrogen. Plasma etching for removing native oxide from the surface of the substrates was performed in a pure Ar ambient at 4 Pa by applying a 600 V, 100 kHz, 10 μs negative pulsed signal to the substrate holder. During the film deposition, the incident energy of the depositing species was controlled by applying a negative pulsed bias voltage (U_B) signal to the substrate holder. The operation frequency of the voltage signal was 100 kHz, whereas the range of U_B was chosen from floating potential, U_{fl} (∼−20 V), to 200 V. Ion energy is expressed by U_B under the assumption of: ion energy = eU_B. The range of U_B from U_{fl} to 200 V thus corresponds to the range of ion energy from eU_{fl} to 200 eV.

Mass densities of the resulting films were determined by performing x-ray reflectometry (XRR) measurements using Cu-K_α ($\lambda = 0.15406$ nm) monochromatic radiation. From the measured XRR curve, the critical angle, θ_c, for the total external reflection was obtained, which was used to calculate the mass density.[5] A simulated curve was generated using the X'pert reflectivity program[25] and was fitted to the measured curve to obtain film thickness as well as to verify the calculated mass density. H content of the films was determined by employing a time-of-flight elastic recoil detection analysis setup using a 32 MeV $^{127}I^{8+}$ beam. The incident angle of the beam with respect to the surface normal was chosen as 67.5°, while the detector was placed at a recoil angle of 45°. A detailed description of the experimental setup can be found elsewhere.[26,27] For the analysis, a reference sample with known H content was used for calibration of the data. Film hardness was measured using a nanoindenter (UMIS-2000, Fischer-Cripps Laboratories) by employing a Berkovich shaped diamond tip. The hardness values were obtained from the indentation data using the Oliver–Pharr method.[28] Film stress was measured *ex situ* using a laser-based wafer-curvature method by employing a multibeam optical stress sensor (k-Space Associates, Inc.). For these measurements, films were deposited on 100 ± 20 μm thick Si (100) substrates, and the curvature of the substrate was measured before and after the film deposition. The stress of the film was calculated from the changes in the substrate curvature by using a modified Stoney equation.[29,30]

In order to investigate the bonding properties of the resulting films, Raman spectroscopy was performed using a Renishaw inVia Raman microscope equipped with an Ar laser of wavelength 514.5 nm. Care was taken to avoid sample damage from the laser exposure, which was 40 μW for 15 s. Two Gaussian peak shapes were fitted to 950–1800 cm^{-1} region, and a linearly increasing background was subtracted.

III. RESULTS AND DISCUSSION

A. Plasma properties

Discharge voltage and current waveforms from a 2% C_2H_2 discharge operated at 3.3 Pa are presented in Fig. 1(a). Discharges operated using other gas phase composition and pressures show similar shape of voltage (not shown here) and current waveforms [Fig. 1(b)].

Overall, lower values of U_D (720 and 632 V at 2 and 3.3 Pa, respectively) were obtained for the 2% C_2H_2 discharges as compared to those of the 0% C_2H_2 (752 and 680 V at 2 and 3.3 Pa, respectively). The changes in U_D levels are in accordance with the changes in I_D since the average power for the discharges was kept constant. Moreover, as seen in Fig. 1(b), the discharge operated in pure inert gas ambient (0% C_2H_2) and at 2 Pa exhibits the smallest peak

value of I_D (~13 A) whereas the discharge containing C_2H_2 and operated at 3.3 Pa exhibits the largest peak value of I_D (~25 A). For both, 0% C_2H_2 and 2% C_2H_2, higher I_D is measured at higher pressures. Larger peak values of I_D when the gas atmosphere contains C_2H_2 at both 2 and 3.3 Pa indicate an increased positive ion flux to the cathode and/or increased secondary electron emission at the target. Such discharge current behavior is supported by the reported discharge current characteristics for reactive and nonreactive HiPIMS processes[31–34] and is believed to be related to strong recycling of process gas ions as the reactive gas flow increases.[32–35]

EEDFs for different discharges are presented in Fig. 2 whereas electron density, n_e, and effective electron temperature, T_{eff}, obtained from the EEDFs are presented in Table I. It should be noted here that due to high noise levels, reliable conclusions from the probe measurements could not be drawn during the pulse-on time. Therefore, the EEDFs recorded during pulse-off time; at 60 μs after the pulse initiation, i.e., 35 μs after the pulse-off, are presented here. For 0% C_2H_2, an increased pressure from 2 to 3.3 Pa does not yield an appreciable change in the EEDFs (Fig. 2) as well as in n_e and T_{eff} (Table I).

The EEDFs are relatively narrow as compared to those at 2% C_2H_2 with their peaks around 1–2 eV. A small but distinct electron population from ~20 to 33 eV is also observed. The distinct (low and high energy) electron populations in EEDFs are often encountered in HiPIMS discharges where the plasma electrons often exhibit bi-Maxwellian energy distributions.[36]

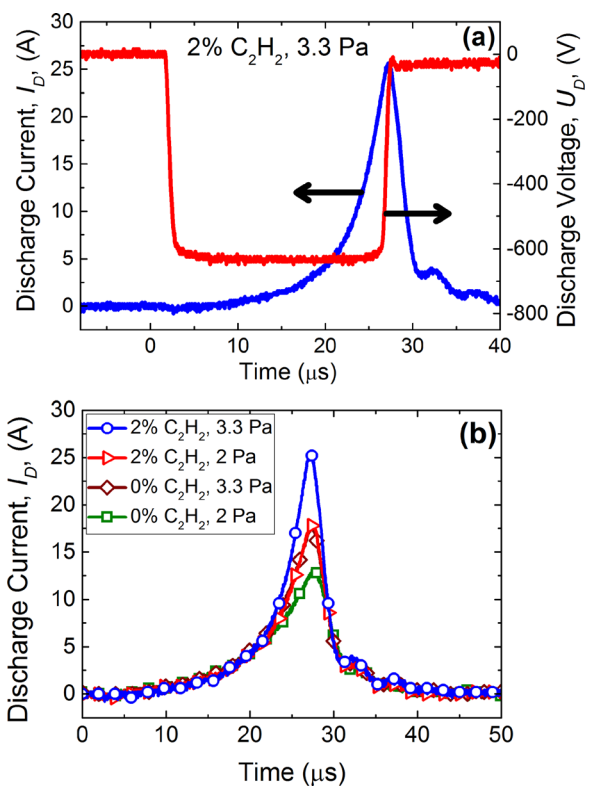

FIG. 1. (Color online) (a) Discharge voltage and current for Ne + Ar discharge and (b) discharge currents for Ne + Ar/C_2H_2 discharges operated using 2% C_2H_2 and at 2 and 3.3 Pa. All discharges were operated using an average power of 42 W.

For 2% C_2H_2 and at 2 Pa, the EEDF is broader as compared to the EEDF for 0% C_2H_2 at the same pressure and exhibits a much more pronounced electron population in the energy range of ~ 20–30 eV. This in turn results in a twofold increase of the mean electron temperature (from 1.4 to 3.3 eV) while n_e remains almost unchanged. A further increase in the discharge pressure to 3.3 Pa leads to an even broader EEDF with majority of the electrons having energies between 2 and 15 eV which corresponds to an T_{eff} of 6.7 eV, i.e., two times higher than the value at 2 Pa.

The results with regards to electron temperature are rather counterintuitive, since (1) higher pressures usually result in reduced electron temperature due to increased probability for ionizing collisions between electrons and gas atoms/molecules and (2) admixing C_2H_2 in the gas atmosphere is expected to further cool down the electrons through dissociation and ionization of hydrocarbon gas molecules. However, an increased electron temperature in a hydrocarbon discharge has been reported by Kim *et al.*[37] where they measured 30% and 35% increase in electron temperatures, respectively, for an Ar/C_2H_2 and Ar/CH_4 discharge as compared to pure Ar discharge. This increase in electron temperature can be understood as follows. The introduction of the reactive C_2H_2 gas into the HiPIMS process leads to the formation of hydrogen ions and hydrogen containing ions. For plasma discharges, various ionizing and dissociating interactions generating $C_xH_y^+$ ionized species and radicals have been reported.[38–40] The electron impact dissociation of C_2H_2 ($C_2H_2 + e^- \rightarrow C_2H + H + e^-$) has a low energy threshold (~7.5 eV)[38] and is therefore likely a dominating interaction, which may result in a substantial amount of C_2H radical generation.[37,38] Electron impact ionization of C_2H_2, which has an energy threshold of 11.4 eV giving $C_2H_2^+$ ions ($C_2H_2 + e^- \rightarrow C_2H_2^+ + 2e^-$),[39] has also been found to be a dominating interaction, especially in high plasma density discharges.[41,42] Other dissociative ionization processes giving C_2H^+, C_2^+, H^+, and C^+ ions[38,43] though have higher energy thresholds in the range of 16–21 eV,[39] may also be possible in a HiPIMS discharge. Therefore, in our Ne + Ar/C_2H_2 discharge, we expect that large amounts of $C_xH_y^+$ ions as well as H^+ ions are generated in addition to C^+, Ne^+, and Ar^+ ions. A

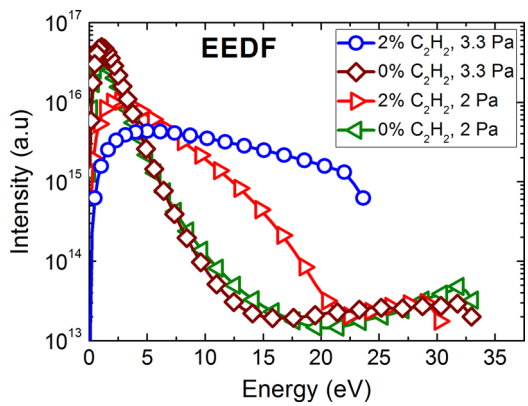

FIG. 2. (Color online) EEDFs for Ne + Ar and Ne + Ar/C_2H_2 discharges operated at 2 and 3.3 Pa using an average power of 42 W. The EEDFs were obtained from plasma current–voltage characteristics measured at 60 μs after the pulse initiation (35 μs after pulse-off).

TABLE I. Plasma parameters determined from plasma current–voltage characteristics measured by using a Langmuir probe at 60 μs after the pulse initiation. The discharges were operated using an average power of 42 W.

Process	Electron density, n_e (m^{-3})	Effective electron temperature T_{eff} (eV)
Ne + Ar (0% C_2H_2), 2 Pa	8.4×10^{16}	1.4
Ne + Ar (0% C_2H_2), 3.3 Pa	1.1×10^{17}	1.3
Ne + Ar (2% C_2H_2), 2 Pa	6.4×10^{16}	3.3
Ne + Ar (2% C_2H_2), 3.3 Pa	6.4×10^{16}	6.7

fraction of these $C_xH_y^+$ ions and H^+ ions bombard the graphite target and modify the target composition. Woods *et al.*[44] have shown that hydrogen ion bombardment increases the secondary electron emission yield (SEEY) of a graphite target. In their case, an increase of almost 30% was detected, but it depends on the amount of hydrogen implanted into the clean graphite target and the bombarding species. It is therefore likely that qualitatively the same trend holds true also in the present HiPIMS case, which also explains the increase in the recorded discharge current when adding C_2H_2 [Fig. 1(b)]. Furthermore, the increased SEEY results in more hot electrons being injected into the volume plasma, since the secondary electrons are accelerated over the cathode sheath potential, which typically is close to the full discharge voltage of about 600–700 V in the present discharges. As a result, the EEDF is broadened toward higher energies, as seen from the Langmuir probe measurements reported in Fig. 2.

In addition, the increase in T_{eff} with increasing pressure is likely due to the increased Ne fraction in the total gas mixture, going from 62% Ne at 2 Pa to 83% Ne at 3.3 Pa. The electron energy has to be sufficiently high to sustain the plasma, which requires more energetic electrons when the Ne content is increased, since Ne has a higher first ionization potential compared to Ar ($E_{i,Ne} = 21.56$ eV and $E_{i,Ar} = 15.76$ eV). Such a strong increase in T_{eff} has also been reported by Haase *et al.*[45] when comparing a pure Ar discharge to a pure Ne discharge in magnetron sputtering.

B. Film properties

Figure 3 presents mass density, H content, and hardness of the resulting films as a function of the negative substrate bias potential, U_B. The films were grown at the discharge conditions described in Sec. II B. With an increase in U_B, the mass density [Fig. 3(a)] and hardness [Fig. 3(c)] exhibit an increase while the H content decreases [Fig. 3(b)]. The increase in mass density and hardness can be attributed to subsurface implantation (also known as subplantation)[2] of the ionized depositing species. Moreover, when synthesized from hydrocarbon based discharges, carbon films are expected to contain large amounts of H due to deposition of C_xH_y species giving rise to C–H bonds. Concurrently, the ion bombardment during the film growth, facilitated by U_B, may lead to C–H bond breaking resulting in reduction of H content of the films.[46,47] The competition between the H incorporation and removal mechanisms outlined above may

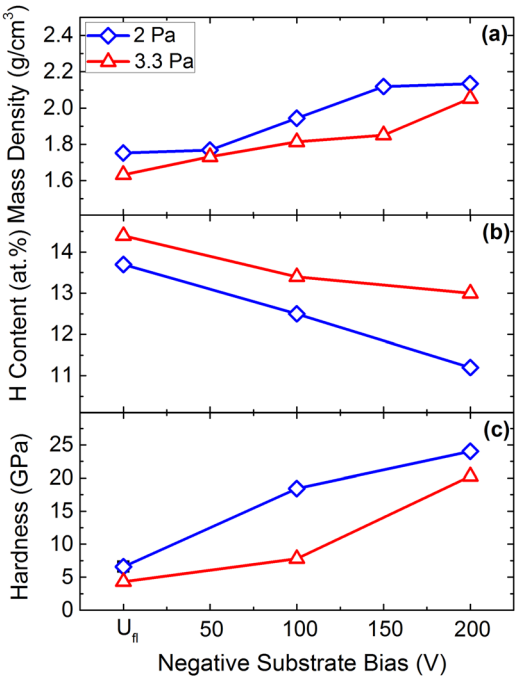

FIG. 3. (Color online) (a) Mass density, (b) H content (at. %) and (c) film hardness as a function of U_B of the films grown using Ne + Ar/C_2H_2 process operated at 2 and 3.3 Pa and an average power of 42 W. Panels (a)–(c) use the same color and symbol coding. The lines are guide for the eye.

also explain the increase in density as well as the decrease in H content observed in Fig. 3.

It is also evident that there is no appreciable difference between the density and hardness values at 2 and 3.3 Pa except for $U_B = 150$ V where a higher mass density and for $U_B = 100$ V where a higher hardness are obtained for the 2 Pa case. However, films grown at a higher pressure of 3.3 Pa contain higher amount of H as compared to those grown at 2 Pa. This is found for all U_B values used. Higher H content of the films at higher pressure of 3.3 Pa could be a consequence of lower bombardment energies of the deposition species due to more collisions in the sheath at the higher pressure of 3.3 Pa. Slight differences in mass densities and hardness at 2 and 3.3 Pa are consistent with the changes in the H content of the films at these pressures. Overall, the H content remained under 15 at. % while the lowest amount of H (close to 11 at. %) is found for the film grown at 2 Pa using maximum value of U_B, i.e., 200 V. Hardness of the films spans a wide range from about 5 to 25 GPa for the range of U_B used. The maximum hardness is about 25 GPa, which is obtained for the film grown at 2 Pa using $U_B = 200$ V.

Increased density and hardness with an increased U_B can either be attributed to an increase in the fraction of C-C sp^3 bonds created via implantation of hyperthermal C ions and/or to an enhanced H removal via C–H bond breaking. In order to elucidate the bonding configuration of the films, Raman spectroscopic measurements were performed, and the results are presented in Fig. 4. The Raman measurements revealed two broad peaks typical for amorphous carbon films in the region of 950–1800 cm^{-1}. The peak centered around 1535–1540 cm^{-1} was assigned to the graphitic peak (G-

peak), whereas the peak centered around 1330–1360 cm^{-1} was assigned to the disorder peak (D-peak).[48] Figure 4 shows the evolution of intensity (height) ratio of the D and G peaks [I(D)/I(G)] and the full-width at half maximum of G-peak (G-width) with respect to U_B. The I(D)/I(G) ratio is proportional to the sp^2 cluster size and inversely proportional to the total (C-H and C-C) sp^3 content.[49] It is found that the I(D)/I(G) is essentially constant with respect to the changes in U_B [Fig. 4(a)] for 2 Pa, whereas a slight increase in I(D)/I(G) with an increase in U_B is observed at the higher pressure of 3.3 Pa. A difference between the I(D)/I(G) ratio for the two pressures is seen for U_B values from U_{fl} to 100 V, whereas at $U_B = 150$ V and $U_B = 200$ V, the ratio is roughly the same for the two pressures.

At 2 Pa, the essentially unchanged I(D)/I(G) ratio with respect to U_B suggests that no major changes in the total sp^3 content occurred. However, since the H content decreased with increased U_B [Fig. 3(b)], it can be concluded that the C-H sp^3 content is likewise decreased, i.e., the C-C sp^3 content must increase. This is consistent with the increase observed in film hardness [Fig. 3(c)] with an increase in U_B. Moreover, Fig. 4(b) shows an overall increase in the G-width from ~170 to ~200 cm^{-1} in the investigated U_B range at both 2 and 3.3 Pa. This increase is associated with bond length and bond angle disorder in a-C films.[48,50] As discussed above, in our films an overall higher sp^3 content is expected with an increase in U_B. This in turn would cause the C-C sp^2 clusters to reduce in size making them more stressed,[50] which is reflected by the increase in G-width. This is consistent with the measured compressive stress in the films which were found to increase with an increase in U_B (not shown here). The overall stress levels, however, were low and did not exceed 0.5 GPa, and the films with thickness in the order of 1 μm were possible to be synthesized without any adhesion layer.

In order to elucidate the effect of admixing Ne in Ar/C_2H_2 discharge, in Figs. 5 and 6, we compare the properties of the films synthesized using Ne + Ar/C_2H_2 process (only from 2 Pa) with the films synthesized in our earlier works under similar process conditions: films synthesized using Ar/C_2H_2, pure Ar and Ne + Ar based HiPIMS discharges.[21,22] Figure 5 shows mass densities of the films resulting from different processes. For the discharge processes operated without C_2H_2, the mass densities are higher as compared to those operated using 2% C_2H_2. This is a direct consequence of H incorporation into the films that lowers the density and film hardness when films are synthesized using hydrocarbon based discharges.[47] Interestingly, the mass densities exhibit different behavior with regards to admixing Ne for the discharges operated with and without C_2H_2. With no C_2H_2, admixing Ne into Ar ambient entails higher mass densities that can be attributed to an increased C ionization via electron temperature enhancement when using Ne. An increased ionization of sputtered C eventually leads to denser a-C films.

For C_2H_2 containing discharges, admixing Ne to Ar/C_2H_2 does not yield any appreciable differences in mass densities. However, a closer inspection of the H contents and hardness values of the corresponding films in Fig. 6 reveals that the films grown using Ne-based discharge contain higher amount of H whereas the lowest and highest achievable film hardness values are comparable. A higher H incorporation in the films indicates that the plasma–chemical interactions produce increased dissociation of C_2H_2 in Ne containing process as compared to Ar. This could be due to higher electron temperatures that have been reported[21] when a discharge is operated using Ne. However, with an increased H content, one expects a reduced mass density and film hardness which is not observed in our case. This could be a consequence of either a different densification route or a different chemical composition of the deposition flux for Ne + Ar/C_2H_2 grown films as compared to Ar/C_2H_2. Densification of DLC:H films may occur through either H removal and subsequent bond rearrangement leading to C–C sp^2 bonds or through subplantation of ionized deposition species giving rise to C–C sp^3 bonds. The latter is observed for ta-C:H films where, as compared to a-C:H films, high hardness and mass densities are obtained with substantially high amount of H (20%–30%) present in the films.[5,51,52]

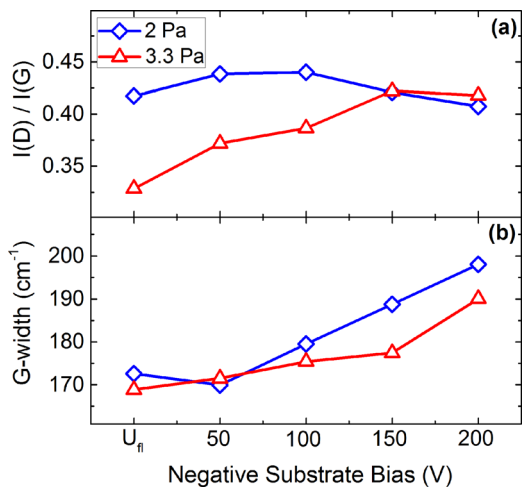

FIG. 4. (Color online) Raman parameters; (a) (intensity) ratio of D and G peaks and (b) G-peak width as a function of U_B of the films grown at 2 and 3.3 Pa of operating pressures and an average power of 42 W. Both panels (a) and (b) use the same color and symbol coding. The lines are guide for the eye only.

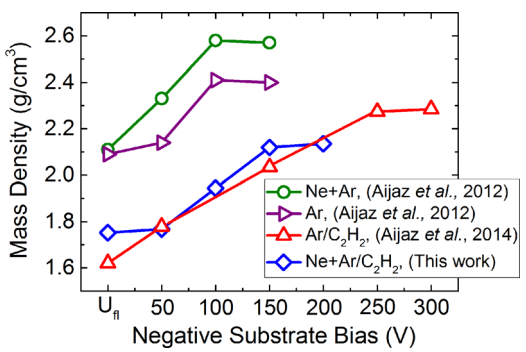

FIG. 5. (Color online) Mass density as a function of U_B of the films grown at 2 Pa using Ne + Ar (Ref. 21), pure Ar (Ref. 21), Ar/C_2H_2 (Ref. 22), and Ne + Ar/C_2H_2 discharges. The lines are guide for the eye only.

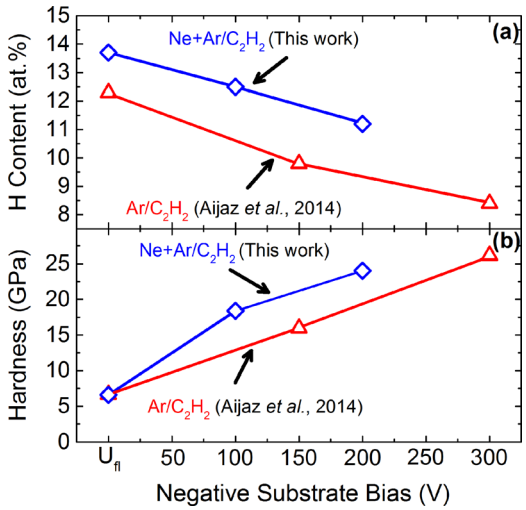

FIG. 6. (Color online) (a) H content and (b) film hardness as a function of U_B of the films grown at 2 Pa using Ar/C_2H_2 (Ref. 22) and $Ne + Ar/C_2H_2$ discharges. The lines are guide for the eye only.

IV. CONCLUSIONS

DLC:H thin films have been synthesized using a $Ne + Ar/C_2H_2$ based HiPIMS discharge process. The discharge properties show that C_2H_2 containing discharges exhibit higher electron temperatures as compared to $Ne + Ar$ discharges. The structural and mechanical properties of the resulting films are found to be governed by the chemistry and energy of the deposition flux. Energetic ion bombardment during the film growth, manipulated by the substrate bias potential, leads to DLC:H films with H content as low as ~11% together with high film hardness that is reaching up to ~25 GPa. The films exhibit low stresses (below 0.5 GPa) that makes it possible to synthesize films with a thickness exceeding 1 μm. The film densification and subsequent changes in the mechanical properties are affected mainly by H removal via ion bombardment.

ACKNOWLEDGMENTS

A.A. and U.H. gratefully acknowledge the financial support provided by the Swedish Research Council (VR) through the Contract Nos. 621-2011-4280 and 621-2014-4882. A.A., T.K., D.L. and U.H. acknowledge the financial support from M-Era.Net (TANDEM). K.S. should like to acknowledge financial support from Linköping University through the "LiU Research Fellows Program, 2011-2015" and the "LiU Career Contract (Dnr-LiU-2015-01510), 2015–2020." S.L. would like to acknowledge the Danish Council for Independent Research, Technology and Production Sciences for financial support. The authors are also grateful for access to the Tandem Laboratory at Uppsala University. European Collaboration in Science and Technology (COST Action MP0804) is gratefully acknowledged for stimulating discussions.

[1]J. Robertson, Diamond Relat. Mater. **4**, 297 (1995).
[2]J. Robertson, Mater. Sci. Eng. R **37**, 129 (2002).
[3]J. K. Luo, Y. Q. Fu, H. R. Le, J. A. Williams, S. M. Spearing, and W. I. Milne, J. Micromech. Microeng. **17**, S147 (2007).
[4]G. Dearnaley and J. H. Arps, Surf. Coat. Technol. **200**, 2518 (2005).
[5]A. C. Ferrari, A. Libassi, B. K. Tanner, V. Stolojan, J. Yuan, L. M. Brown, S. E. Rodil, and B. Kleinsorge, Phys. Rev. B **62**, 11089 (2000).
[6]G. A. Abbas, S. S. Roy, P. Papakonstantinou, and J. A. McLaughlin, Carbon **43**, 303 (2005).
[7]P. Patsalas, S. Kaziannis, C. Kosmidis, D. Papadimitriou, G. Abadias, and G. A. Evangelakis, J. Appl. Phys. **101**, 124903 (2007).
[8]M. Pervolaraki, P. Komninou, J. Kioseoglou, A. Othonos, and J. Giapintzakis, Appl. Surf. Sci. **278**, 101 (2013).
[9]M. Samuelsson, K. Sarakinos, H. Högberg, E. Lewin, U. Jansson, B. Wälivaara, H. Ljungcrantz, and U. Helmersson, Surf. Coat. Technol. **206**, 2396 (2012).
[10]U. Helmersson, M. Lattemann, J. Bohlmark, A. P. Ehiasarian, and J. T. Gudmundsson, Thin Solid Films **513**, 1 (2006).
[11]D. Lundin and K. Sarakinos, J. Mater. Res. **27**, 780 (2012).
[12]J. T. Gudmundsson, N. Brenning, D. Lundin, and U. Helmersson, J. Vac. Sci. Technol., A **30**, 030801 (2012).
[13]K. Sarakinos, A. Braun, C. Zilkens, S. Mráz, J. M. Schneider, H. Zoubos, and P. Patsalas, Surf. Coat. Technol. **206**, 2706 (2012).
[14]B. M. Dekoven *et al.*, *46th Annual Technical Conference Proceedings* (2003), p. 158.
[15]M. Lattemann, B. Abendroth, A. Moafi, D. G. McCulloch, and D. R. McKenzie, Diamond Relat. Mater. **20**, 68 (2011).
[16]J. Lin, W. D. Sproul, R. Wei, and R. Chistyakov, Surf. Coat. Technol. **258**, 1212 (2014).
[17]S. Nakao, K. Yukimura, S. Nakano, and H. Ogiso, IEEE Trans. Plasma Sci. **41**, 1819 (2013).
[18]T. Kimura and H. Kamata, Jpn. J. Appl. Phys., Part 1 **55**, 07LE02 (2016).
[19]J. Bohlmark, J. Alami, C. Christou, A. P. Ehiasarian, and U. Helmersson, J. Vac. Sci. Technol., A **23**, 18 (2005).
[20]T. Kubart, M. Čada, D. Lundin, and Z. Hubička, Surf. Coat. Technol. **238**, 152 (2014).
[21]A. Aijaz, K. Sarakinos, D. Lundin, N. Brenning, and U. Helmersson, Diamond Relat. Mater. **23**, 1 (2012).
[22]A. Aijaz, K. Sarakinos, M. Raza, J. Jensen, and U. Helmersson, Diamond Relat. Mater. **44**, 117 (2014).
[23]M. A. Lieberman, *Principles of Plasma Discharges and Materials Processing*, 2nd ed. (Willey, Hoboken, NJ, 2005).
[24]F. Magnus and J. T. Gudmundsson, Rev. Sci. Instrum. **79**, 073503 (2008).
[25]*PANalytical, X'Pert Reflectivity* (PANalytical B.V., Almelo, The Netherlands, 2012).
[26]J. Jensen, D. Martin, A. Surpi, and T. Kubart, Nucl. Instrum. Methods Phys. Res., Sect. B **268**, 1893 (2010).
[27]H. J. Whitlow, G. Possnert, and C. S. Petersson, Nucl. Instrum. Methods Phys. Res., Sect. B **27**, 448 (1987).
[28]W. C. Oliver and G. M. Pharr, J. Mater. Res. **7**, 1564 (1992).
[29]G. G. Stoney, Proc. R. Soc. London, Ser. A **82**, 172 (1909).
[30]G. C. A. M. Janssen, M. M. Abdalla, F. van Keulen, B. R. Pujada, and B. van Venrooy, Thin Solid Films **517**, 1858 (2009).
[31]D. Lundin, N. Brenning, D. Jädernäs, P. Larsson, E. Wallin, M. Lattemann, M. A. Raadu, and U. Helmersson, Plasma Sources Sci. Technol. **18**, 045008 (2009).
[32]F. Magnus, T. K. Tryggvason, S. Olafsson, and J. T. Gudmundsson, J. Vac. Sci. Technol., A **30**, 050601 (2012).
[33]F. Magnus, O. B. Sveinsson, S. Olafsson, and J. T. Gudmundsson, J. Appl. Phys. **110**, 083306 (2011).
[34]M. Aiempanakit, A. Aijaz, D. Lundin, U. Helmersson, and T. Kubart, J. Appl. Phys. **113**, 133302 (2013).
[35]J. T. Gudmundsson, D. Lundin, N. Brenning, M. A. Raadu, C. Huo, and T. M. Minea, "An ionization region model of the reactive Ar/O_2 high power impulse magnetron sputtering discharge," Plasma Sources Sci. Technol. (submitted).
[36]J. T. Gudmundsson, J. Alami, and U. Helmersson, Surf. Coatings Technol. **161**, 249 (2002).
[37]B. K. Kim and T. A. Grotjohn, Diamond Relat. Mater. **9**, 37 (2000).
[38]J. Benedikt, J. Phys. D: Appl. Phys. **43**, 043001 (2010).
[39]K. De Bleecker, A. Bogaerts, and W. Goedheer, Phys. Rev. E **73**, 026405 (2006).
[40]Y. H. Cheng, Y. P. Wu, J. G. Chen, X. L. Qiao, C. S. Xie, B. K. Tay, S. P. Lau, and X. Shi, Surf. Coat. Technol. **135**, 27 (2000).

[41]M. Weiler, S. Sattel, T. Giessen, K. Jung, and H. Ehrhardt, Phys. Rev. B **53**, 1594 (1996).
[42]A. Baby, C. M. O. Mahony, and P. D. Maguire, Plasma Sources Sci. Technol. **20**, 015003 (2011).
[43]J. R. Doyle, J. Appl. Phys. **82**, 4763 (1997).
[44]M. E. Woods, B. J. Hopkins, G. F. Matthews, G. M. McCracken, P. M. Sewell, and H. Fahrang, J. Phys. D: Appl. Phys. **20**, 1136 (1987).
[45]F. Haase, D. Lundin, S. Bornholdt, and H. Kersten, Contrib. Plasma Phys. **55**, 701 (2015).
[46]W. Jacob, Thin Solid Films **326**, 1 (1998).
[47]J. Benedikt, R. V. Woen, S. L. M. Van Mensfoort, V. Perina, J. Hong, and M. C. M. Van De Sanden, Diamond Relat. Mater. **12**, 90 (2003).
[48]C. Casiraghi, A. C. Ferrari, and J. Robertson, Phys. Rev. B **72**, 085401 (2005).
[49]M. A. Tamor and W. C. Vassell, J. Appl. Phys. **76**, 3823 (1994).
[50]K. W. R. Gilkes, S. Prawer, K. W. Nugent, J. Robertson, H. S. Sands, Y. Lifshitz, and X. Shi, J. Appl. Phys. **87**, 7283 (2000).
[51]M. Weiler, K. Lang, E. Li, and J. Robertson, Appl. Phys. Lett. **72**, 1314 (1998).
[52]P. Koidl, C. Wild, B. Dischler, J. Wagner, and M. Ramsteiner, Mater. Sci. Forum **52–53**, 41 (1990).